(22) F. G. Mann, *J. Chem. Soc.*, 461 (1934).
(23) G. W. Watt and W. A. Cude, *J. Am. Chem. Soc.*, **90**, 6382 (1968).
(24) Stanley E. Livingstone, "Comprehensive Inorganic Chemistry", Vol. 3, A. F. Trotman-Dickenson, Ed., Pergamon, New York, N.Y., 1973, p 1352.
(25) See, for example, C. M. Harris, R. S. Nyholm, and N. C. Stephenson, *Nature (London)*, **177**, 1127 (1956); C. M. Harris and N. C. Stephenson, *Chem. Ind. (London)*, 426 (1957).

Optical Spectra and the Free-Volume Model for the Transport Behavior of Glass-Forming Melts

N. Islam,* M. R. Islam, S. Ahmad, and B. Waris

Contribution from the Department of Chemistry, Aligarh Muslim University, Aligarh 202001, India. *Received July 29, 1974*

Abstract: The optical spectra of MX_2 (M = Mn, Co, and Ni; X = Cl and Br) -rich mixtures of $R_4B^+X^-$ (R = propyl, butyl, pentyl, hexyl, heptyl, and octyl, and is either the same or different; B = N and P; and X = Cl, Br, and I) have been identified as due to the presence of tetrahedral, T_d tetrahalometalate(II) ions, MX_4^{2-}. The band assignments of NiX_4^{2-} have been made by constructing the energy level diagrams for the d^8 configuration in a cubic T_d field based on the four ligand-field (LF) parameters. These parameters for $NiCl_2X_2^{2-}$ have been taken as approximately averages of those of $NiCl_4^{2-}$ and NiX_4^{2-}. The optical electronegativity of nickel(II), $OE_{[Ni(II)]}$, has been computed from the corresponding LF parameters and the low-energy charge-transfer (CT) spectrum and is found to be 2.1. The CT spectra of X^- in MX_2-rich mixtures of $R_4N^+X^-$ have been found to be unaffected by the low conducting and highly viscous medium containing the species, $\{(R_4N^+)_2MX_4^{2-}\}_x$ and may be due to the transitions to $np^5\gamma_i$ configuration. The free volume model has been found suitable in explaining the transport behavior of glass-forming melts as supported by almost identical secondary glass transition temperatures, $T_{0,A}$ and $T_{0,\phi}$ for $MnCl_4^{2-}$, $CoCl_4^{2-}$, and $NiCl_4^{2-}$ as 277.23 ± 1.27, 276.60 ± 0.40, and 269.43 ± 2.17°K, respectively, and also by several linear plots.

Tetrahedral tetrahalometalates have been reported[1-9] in the low-melting organic halides of large [cation]/[anion] ratio. The metal halide-rich mixtures containing $(R_4B^+)_2MX_4^{2-}$ have been found to supercool to glassy states.[5]

The present work deals with the optical spectra of MX_2-rich mixtures of $R_4B^+X^-$ [$(C_4H_9)_4N^+Cl^-$, $(C_4H_9)_4P^+Br^-$, $(C_4H_9)_4N^+Br^-$, $(C_8H_{17})_3C_3H_7N^+Br^-$, $(C_4H_9)_4N^+I^-$, $(C_5H_{11})_4N^+I^-$, $(C_6H_{13})_4N^+I^-$, $(C_7H_{15})_4N^+I^-$, and $(C_4H_9)_3C_3H_7N^+I^-$0 and their comparison with those in the corresponding dilute solutions. The CT and the LF bands of CoX_4^{2-} and NiX_4^{2-} are recorded. The band assignments of the latter have been made by constructing the energy level diagrams[10] based on the four LF parameters and comparing them with those recorded for NiX_4^{2-} and $NiCl_2X_2^{2-}$, i.e., $NiCl_4^{2-}$, $NiBr_4^{2-}$, $NiCl_2Br_2^{2-}$ and $NiCl_2I_2^{2-}$. The CT spectra of X^- in MX_2-rich mixtures of $R_4N^+X^-$ have also been recorded.

The electrical conductances, densities, and viscosities of MCl_2 in molten $(C_4H_9)_4N^+Cl^-$ have been measured at several temperatures and those of $CoCl_2$ in $(C_4H_9)_4N^+I^-$ as functions of composition and temperature. The applicability of the free-volume model[11-17] in explaining the transport behavior of the glass-forming melts has been examined.

Experimental Section

Tetra-*n*-alkylammonium (Fluka and Eastman) and phosphonium (Alfa Inorganics) halides, $R_4B^+X^-$, were used as solvents in the molten state. Anhydrous metal chlorides, MCl_2, were prepared[18,19] from their recrystallized hydrated salts (E. Merck) while $NiBr_2$ was obtained commercially. The spectra of MX_2 in molten $R_4B^+X^-$ were recorded on digitalized Cary Model 14 and Beckman Model DK-2A spectrophotometers.

Electrical conductances were measured with a Philips-PR9500 conductivity bridge at 50 Hz using calibrated capillary type conductivity cells. The dielectric constant was measured with a Sargent Chemical Oscillometer Model V. The capacitive effect of electrolyte-electrode double layer being of the order of 10^{-4} pF has been neglected. Density measurements were made in a dilatometer calibrated for 0.005 ml at several temperatures with ±0.3% accuracy. The viscosities were measured in a calibrated Ubbelohde capillary viscometer with an accuracy of ±0.1 to 2.5%. Preparation of the samples and the above measurements were carried out in an inert atmosphere in a relay controlled thermostated oil bath of ±0.1 and ±0.2° thermal stabilities over 0 to 100 and 100 to 200°, respectively.

The energy level diagrams for NiX_4^{2-} were constructed[1,10] by computing the energy levels on an IBM-1130 computer.

Results and Discussion

I. Optical Spectra. Ligand-Field Transitions. The optical spectra of NiX_2 + $R_4B^+X^-$ have been identified as due to the presence of T_d NiX_4^{2-} on the basis of their comparison with those reported earlier.[1] The LF spectra of $NiCl_4^{2-}$, $NiBr_4^{2-}$, $NiCl_2Br_2^{2-}$, and $NiCl_2I_2^{2-}$ have been fitted to their respective energy level diagrams and the assignments of the bands have been made.

A. $NiCl_2$ + $R_4N^+Cl^-$. The d-d spectra of $NiCl_2$ in molten $(C_4H_9)_4N^+Cl^-$ consist of an intense band with peaks at 14,280 and 15,380 cm^{-1} and a shoulder at ~16,660 cm^{-1}, and a broad band with a peak at ~7500 cm^{-1}. It is apparent from the energy level diagram (Figure 1) that three transitions are spin allowed, two of which are orbital transitions, $\Gamma_{2,5}:{}^3T_2(F) \leftarrow \Gamma_1:{}^3T_1(F)$, and $\Gamma_5:{}^3A_2(F) \leftarrow \Gamma_1:{}^3T_1(F)$, and the third one is due to $\Gamma_5:{}^3T_1(P) \leftarrow \Gamma_1:{}^3T_1(F)$ transitions. The first transition reported[1] at ~4000 cm^{-1} has not been recorded due to the overlapping region of the solvent. The remaining two transitions have been reported by several authors[1,20-24] and agree with those found in the present case at ~7500 and 14,280 cm^{-1}.

In spite of its inherent limitations[25] the LF theory rationalizes the spectrum satisfactorily. However, it does not seem to account for the little details of the band, ${}^3T_1(P) \leftarrow {}^3T_1(F)$, as predicted by the theory for $\Gamma_3:{}^3T_1(P) \leftarrow \Gamma_1:{}^3T_1(F)$, $\Gamma_4:{}^3T_1(P) \leftarrow \Gamma_1:{}^3T_1(F)$, and $\Gamma_1:{}^3T_1(P) \leftarrow \Gamma_1:{}^3T_1(F)$ transitions at 14,340, 14,650, and 14,840 cm^{-1},

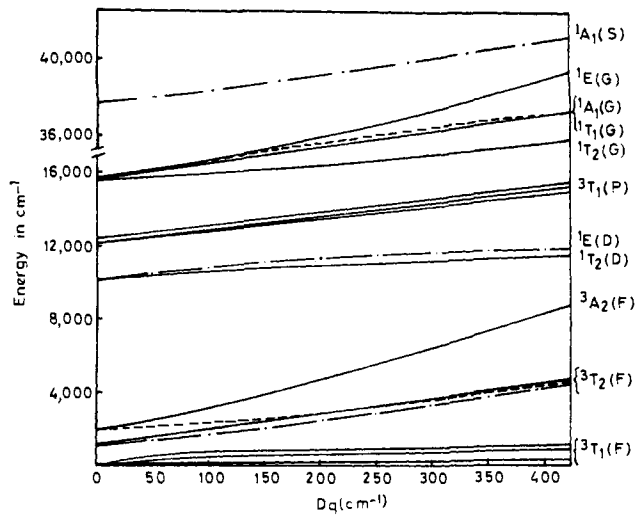

Figure 1. Energy level diagram for $NiCl_4^{2-}$ in molten $(C_4H_9)_4N^+Cl^-$ ($\lambda = -275$, $B = 740$, and $C/B = 3.97$ cm^{-1}). The computed electronic levels were matched closely with those of the observed bands at ~7,500 and 14,280 cm^{-1} for Γ_5:$^3A_2(F) \leftarrow \Gamma_1$:$^3T_1(F)$ and Γ_5:$^3T_1(P) \leftarrow \Gamma_1$:$^3T_1(F)$ transitions, respectively.

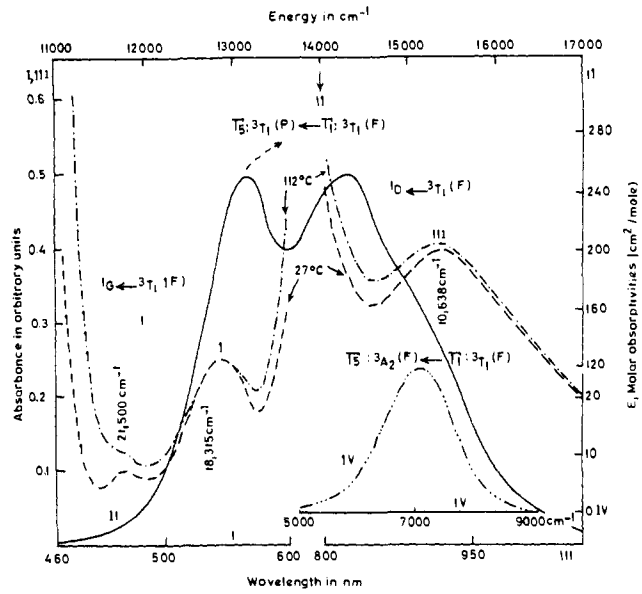

Figure 2. Spin-forbidden (I and III at 27 and 112°) and spin-allowed (II and IV at 112°) ligand-field spectra of tetrabromonickelate(II) ions in molten $(C_4H_9)_4P^+Br^-$.

respectively, while the experimental result corresponds to an intense band at 15,380 and a shoulder at ~16,660 cm^{-1}. The latter is close to the computed energy for Γ_5:$^1T_2(G) \leftarrow \Gamma_1$:$^3T_1(F)$ transitions. It appears that the close proximity of the intense band for Γ_5:$^3T_1(P) \leftarrow \Gamma_1$:$^3T_1(F)$ transitions and those of weak ^1G states renders the actual band positions to shift toward a position determined by the relative intensity of several closely lying overlapping Gaussians, also enveloping some of the extremely weak components. It therefore appears reasonable to assign the band at 14,280 cm^{-1} to Γ_5: $^3T_1(P) \leftarrow \Gamma_1$:$^3T_1(F)$ transitions enveloping the components predicted at 14,340 and 14,650 for transitions to Γ_3:$^3T_1(P)$ and Γ_4:$^3T_1(P)$ levels, respectively, and the band at 15,380 cm^{-1} to Γ_1:$^3T_1(P) \leftarrow \Gamma_1$:$^3T_1(F)$ transitions. However, all three components, i.e., 14,280, 15,380, and ~16,660 cm^{-1}, of the intense band are to be considered for the estimation of the oscillator strength as the intensity of the latter shoulder appears to have been borrowed from the ^3P state.

B. $NiBr_2 + R_4P^+Br^-$. The LF spectrum of $NiBr_2$ in molten $(C_4H_9)_4P^+Br^-$ consists of two weak bands at 18,315 and 21,500 cm^{-1}, an intense band with peaks at 13,200 and 14,200, and a shoulder at ~15,000 cm^{-1}, followed by a weak band at 10,640 cm^{-1} and a shoulder at ~9850 cm^{-1}, and a broad band at ~7040 cm^{-1} (Figure 2).

The spectrum is analyzed as cited above. The computed electronic levels were matched with those of the experimental bands at ~7,040, ~10,000, ~10,600, and 13,200 cm^{-1} corresponding to Γ_5:$^3A_2(F) \leftarrow \Gamma_1$:$^3T_1(F)$, Γ_5:$^1T_2(D) \leftarrow \Gamma_1$:$^3T_1(F)$, Γ_3:$^1E(D) \leftarrow \Gamma_1$:$^3T_1(F)$, and Γ_5:$^3T_1(P) \leftarrow \Gamma_1$:$^3T_1(F)$ transitions, respectively.

In addition to the limitations of the LF theory cited above, the predicted energies for the four components of ^1G state, i.e., Γ_5:$^1T_2(G) \leftarrow \Gamma_1$:$^3T_1(F)$, Γ_4:$^1T_1(G) \leftarrow \Gamma_1$:$^3T_1(F)$, Γ_1:$^1A_1(G) \leftarrow \Gamma_1$:$^3T_1(F)$, and Γ_3:$^1E(G) \leftarrow \Gamma_1$:$^3T_1(F)$ transitions at 15,780, 17,085, 17,205, and 18,540 cm^{-1}, are unaccounted for in a true sense as only two bands are obtained at 18,315 and 21,500 cm^{-1}, respectively. The band at 18,315 cm^{-1} is clearly a transition to a ^1G state as it lies very close to that predicted for the Γ_3:$^1E(G)$ level but the theory is expected to underestimate the overall positions of the ^1G bands by an appreciable amount, and thus the band at 21,500 cm^{-1} is unaccounted for.

The second part of this section deals with the absorption spectra of $NiBr_2$-rich mixtures of molten $(C_4H_9)_4P^+Br^-$. Upon increasing the $[NiBr_2]$ to near stoichiometric point, the ratio of $[NiBr_4^{2-}]$ to $[Br^-]$ increases rapidly and the melt containing $(R_4B^+)_2NiX_4^{2-}$ supercools to a glassy material. It is interesting to note that the thin film spectrum of the glassy material has been found similar to those in the corresponding dilute solutions. Beer's law has been found to be obeyed in fairly concentrated solutions. This indicates the presence of the same absorbing species in the two cases.

The shoulder at ~21,500 cm^{-1} appeared as a distinct peak in the glassy material at 27° and the weak band at 10,640 cm^{-1} became somewhat narrower (Figure 2). The absorbance of all the bands increased and the bandwidth near the foot of the band decreased on cooling the concentrated melt. For example, the absorbance increased by ~15% in $NiBr_4^{2-}$ at the band maximum while the bandwidth decreased by ~33 cm^{-1} near 16,660 cm^{-1} on lowering the temperature from 112 to 27°. This phenomenon is similar in dilute as well as in concentrated solutions which supercool to glassy states. The reasons for such behaviors are associated with the creation of holes or an increase in the free volume (cf. transport behavior) which in turn lowers the density of the absorbing species as well as an increase in the vibronic interaction with successive increases in temperature.

The oscillator strengths of ν_2, Γ_5:$^3A_2(F) \leftarrow \Gamma_1$:$^3T_1(F)$, and ν_3, Γ_5:$^3T_1(P) \leftarrow \Gamma_1$:$^3T_1(F)$, transition bands of $NiBr_4^{2-}$ have been obtained as 1.7×10^{-4} and 31×10^{-4}, respectively. Their ratio, $f(\nu_3)/f(\nu_2)$, at 112 and 27° is ~18.24. This implies that there was no perceptible change in the character of Ni^{2+}–Br^- bonds in the above temperature intervals.

In view of the above results, the spin-allowed bands of $NiCl_2X_2^{2-}$ have been recorded in the corresponding thin films, as their T_d geometry remains unaltered by successive increases in $[MCl_2]$ until the glassy materials are obtained.

C. $NiCl_2 + R_4N^+X^-$ (X = Br or I). Thin film spectra of $NiCl_2$ in several organic bromides and iodides consist of bands similar to those cited above for Γ_5:$^3A_2(F) \leftarrow \Gamma_1$:$^3T_1(F)$ and Γ_5:$^3T_1(P) \leftarrow \Gamma_1$:$^3T_1(F)$ transitions. The LF parameters used in the computation of energy levels for the corresponding diagrams of $NiCl_2X_2^{2-}$ have been taken as

Table I. Band Positions for NiX_4^{2-} (cm^{-1})

Transitions	Band positions for $NiCl_2Br_2^{2-}$: Predicted ≈ averages of those of $NiCl_4^{2-}$ + $NiBr_4^{2-}$	Obsd	Band positions for $NiCl_2I^{2-}$: Predicted ≈ averages of those of $NiCl_4^{2-}$ + NiI_4^{2-}	Obsd
$^3T_1(P) \leftarrow {}^3T_1(F)$	13,740	13,800	12,810	12,820
$^3T_1(P) \leftarrow {}^3T_1(F)$	14,790	14,600	13,765	13,417
$^3A_2(F) \leftarrow {}^3T_1(F)$	~7,270	~7,240	~7,275	~7,270

Table II. LF Parameters for NiX_4^{2-} (cm^{-1})

Parameters	$NiCl_4^{2-}$	$NiBr_4^{2-}$	NiI_4^{2-}	$NiCl_2Br_2^{2-}$	$NiCl_2I_2^{2-}$
B	740	680	537	710	638.5
C/B	3.97	3.88	5.51	3.92	4.74
Dq	358	332	331	345	344.5

Table III. Computed[a] Band Positions for NiX_4^{2-} (cm^{-1})

Transitions	$NiCl_2Br_2^{2-}$	$NiCl_2I_2^{2-}$
$\Gamma_5: {}^3A_2(F) \leftarrow \Gamma_1: {}^3T_1(F)$	7,290	7,300
$\Gamma_5: {}^3T_1(P) \leftarrow \Gamma_1: {}^3T_1(F)$	13,790	12,790

[a] $NiCl_2Br_2^{2-}$: $\lambda = -275$, $B = 713.75$, $C/B = 3.93$, $Dq = 345$. $NiCl_2I_2^{2-}$: $\lambda = -275$, $B = 639.75$, $C/B = 4.7$, and $Dq = 345$ cm^{-1}.

averages of those of $NiCl_4^{2-}$ and NiX_4^{2-} as supported by the following consideration.

The dilute solutions of $NiCl_2$ or $NiBr_2$ and $NiCl_2$ or NiI_2 in several molten bromides and iodides, respectively, yield essentially the same spectra as those of $NiBr_4^{2-}$ and NiI_4^{2-}. On the other hand, the absorbing species in $NiCl_2$-rich mixtures of molten $R_4N^+X^-$ have been identified as $NiCl_2X_2^{2-}$ on the basis of the following comparison (Table I). Thus it may be assumed that each metal ion in the glassy material is essentially present in a T_d field of two chloride and two bromide or iodide ions (Table II). The best fitted values are taken as approximately close to those which describe the experimental results (Table III). A comparison of these computed energy levels as well as the predicted band positions (Table I) based on the averages of those of $NiCl_4^{2-}$ and NiX_4^{2-} for $NiCl_2X_2^{2-}$ with the experimental band positions reinforces the above deductions for the LF parameters. Similarly MX_2-rich mixtures of molten $R_4B^+X^-$ result in $(R_4B^+)_2MX_4^{2-}$ unlike those in dilute solutions. Such species are expected to be weakly dissociated and at the same time highly viscous. The transport behavior is therefore examined later.

D. $CoX_2 + R_4N^+X^-$. The spectra of CoX_2-rich mixtures of $R_4N^+X^-$ consist of a broad band with structure located between 6660 and 4000 cm^{-1} and an intense resolved band which extends from 16,660 to ~12,000 cm^{-1} may be assigned to $^4T_1(F) \leftarrow {}^4A_2(F)$ and $^4T_1(P) \leftarrow {}^4A_2(F)$ transitions,[3,24,26-29] respectively. The latter has also some contributions from ^2G due to overlapping. The LF spectra of CoX_4^{2-} in several systems are summarized in Table IV.

E. $MnX_2 + R_4N^+X^-$. The visible spectrum of MnX_4^{2-} has not been obtained in thin films because of their low intensity as all of the LF transitions are spin forbidden. A band has been recorded in the ultraviolet region at 37,740 cm^{-1} which resembles one of the bands reported for MnX_4^{2-}. T_d geometry may be assumed for the absorbing species in $MnX_2 + R_4N^+X^-$ on the basis of those reported[30] for $MnBr_2 + R_4P^+Br^-$.

Charge-Transfer Spectra of MX_4^{2-}. The CT spectra of MX_4^{2-} recorded in the ultraviolet region (Table V) suggest a predominant covalent character in the metal–ligand bond.[3]

The CT transition is attributed[1] to an electron jump from a filled γ_4 subshell to the partially filled γ_5 subshell. The γ_4 subshell has π-type two-center symmetry and is nonbonding in metal–ligand directions in the LCAO-MO model that ignores metal orbitals above 4p. The lowest energy CT band has been employed in calculating the optical electronegativity, OE, of nickel(II) relative to the γ_4 subshell. Jørgensen[31] has associated this quantity with the electron bonding. The basic relation in OE is given by the relation, $\nu_{corr} = 3 \times 10^4(OE_{[X]} - OE_{[M]})$, where ν_{corr} and 3×10^4 stand for the corrected transition energy and the conversion factor of Pauling electronegativity scale to reciprocal centimeters, respectively. The ν_{corr} is given by

$$\nu_{corr} = \nu_{obsd} - 10Dq + D[\langle S(S+1) - S(S+1)\rangle]$$

where the bracketed term is $-\frac{2}{3}$ for Ni(II) ions and D is the spin-pairing energy parameter obtained from the LF parameters as shown by the relation $D = (\frac{7}{6})[(\frac{5}{2})B + C]$. The low-energy CT bands of $NiCl_2X_2^{2-}$ taken as the averages of ν_{obsd} for $NiCl_4^{2-}$ and NiX_4^{2-} are supported by the same $OE_{[Ni(II)]}$ viz. 2.1 obtained in all the five cases (Table VI). This fits well with Jørgensen's correlation.[32] The shift of bands toward lower energies in the order $NiCl_4^{2-}$ >

Table V. CT Bands of MX_4^{2-} (cm^{-1})

$CoCl_4^{2-}$ in $R_4N^+Cl^-$	$CoCl_2Br_2^{2-}$ in $R_4N^+Br^-$	$CoCl_2I_2^{2-}$ in $R_4N^+I^-$	$NiCl_4^{2-}$ in $R_4N^+Cl^-$	$NiCl_2Br_2^{2-}$ in $R_4N^+Br^-$	$NiBr_4^{2-}$ in $R_4P^+Br^-$
42,735	~35,460 (sh)	30,030	35,460	~31,950	28,409
46,083	37,735	32,786	38,460		30,303
			42,550		34,480
					37,175

Table IV. Band Positions of CoX_4^{2-} (cm^{-1})

Systems	$^4T_1(F) \leftarrow {}^4A_2(F)$				$^4T_1(P) \leftarrow {}^4A_2(F)$			
$CoCl_2 + (C_4H_9)_4N^+Cl^-$					14,490	15,150	16,000	16,390
$CoCl_2 + (C_8H_{17})_3C_3H_7N^+Br^-$	4444	5154		5714	13,986	14,285	15,479	
	4376							
	4282							
$CoCl_2 + (C_4H_9)_4N^+I^-$	4405	5263	5405	5571 (sh)	13,157	13,793	14,184	~15,503 (sh)
$CoCl_2 + (C_5H_{11})_4N^+I^-$	4424	5128	~5279 (sh)		13,157	13,698	14,285	~15,384 (sh)
$CoCl_2 + (C_6H_{13})_4N^+I^-$					13,245	13,947	~14,492 (sh)	
$CoCl_2 + (C_7H_{15})_4N^+I^-$	4424	5167	5464	5714	~13,245 (sh)	13,698	14,084	14,492
	4347							15,625
	4273							

Table VI. Optical Electronegativities Obtained from CT Spectra and the LF Parameters

Absorbing species	Parameters in cm^{-1}		Parameters in Pauling units of 3×10^4 cm^{-1}					
	B	C	$10Dq$	$^2/_3D$	ν_{obsd}	ν_{corr}	$OE_{[X]}$	$OE_{[Ni(II)]}$
$NiCl_4^{2-}$	740	2938	0.119	−0.124	1.184	0.939	3.0	2.06
$NiCl_2Br_2^{2-}$	713.75	2805	0.112	−0.118	~1.065[a]	0.832	2.9[a]	2.07
$NiBr_4^{2-}$	680	2638	0.11	−0.112	0.947	0.725	2.8	2.08
$NiCl_2I_2^{2-}$	639.75	3007	0.112	−0.118	~0.798[a]	0.568	2.65[a]	2.08
NiI_4^{2-}	537	2959	0.11	−0.115	0.65[b]	0.425	2.5	2.08

[a] ν_{obsd} and $OE_{[X]}$ for $NiCl_2X_2^{2-}$ are taken as averages of those of $NiCl_4^{2-}$ and NiX_4^{2-}. [b] Reference 1.

Table VII. Computer-Fitted Least-Squares Representation for Specific and Equivalent Conductances[a] and Fluidities[b] as a Function of Temperature[c] for MX_2-Rich Mixtures of Molten $R_4N^+X^-$

System	Equation no.	a		b		c		Std Dev in k, Λ/ϕ
		k or Λ	ϕ	k or Λ	ϕ	k or Λ	ϕ	
$(C_4H_9)_4N^+Cl^-$ + $MnCl_2$	(i)	0.1789×10^{-2}	3.3487	-0.4223×10^{-4}	−0.07901	0.2622×10^{-6}	0.4662×10^{-3}	0.025 ± 0.005
(24.5 mol %)	(ii)	0.2367	36.226	923.8	295.03	243.4	321.75	0.025 ± 0.005
	(iii)	382.5	5226.0	605.1	712.68	278.5	275.96	0.012 ± 0.006
$(C_4H_9)_4N^+Cl^-$ + $CoCl_2$	(i)	0.1386×10^{-2}	5.4064	-0.3143×10^{-4}	−0.10124	0.184×10^{-6}	0.4869×10^{-3}	0.015 ± 0.005
(26.6 mol %)	(ii)	0.0947	198.97	743.1	682.08	267.2	290.08	0.015 ± 0.005
	(iii)	210.3	12737.0	617.8	916.17	277.0	276.21	0.012 ± 0.008
$(C_4H_9)_4N^+Cl^-$ + $NiCl_2$	(i)	0.0708×10^{-2}	3.9199	-0.1783×10^{-4}	−0.08283	0.1158×10^{-6}	0.4442×10^{-3}	0.02
(22.1 mol %)	(ii)	0.0551	69.24	663.63	437.02	272.10	309.13	0.02
	(iii)	160.2	8377.8	621.7	875.01	271.6	267.26	0.01 ± 0.006

[a] Temperature range for conductance: 373–413 °K. [b] Temperature range for fluidity: Mn^{2+}, 393–428 °K; Co^{2+}, 398–433 °K, and Ni^{2+}, 393–428 °K. [c] t, °C, T, °K. (i) $Y = a + bt + ct^2$; (ii) $Y = a \exp[-b/(T - c)]$; and (iii) $Y = aT^{-1/2} \exp[-b/(T - c)]$ in which c corresponds to $T_0(\Lambda, \phi)$.

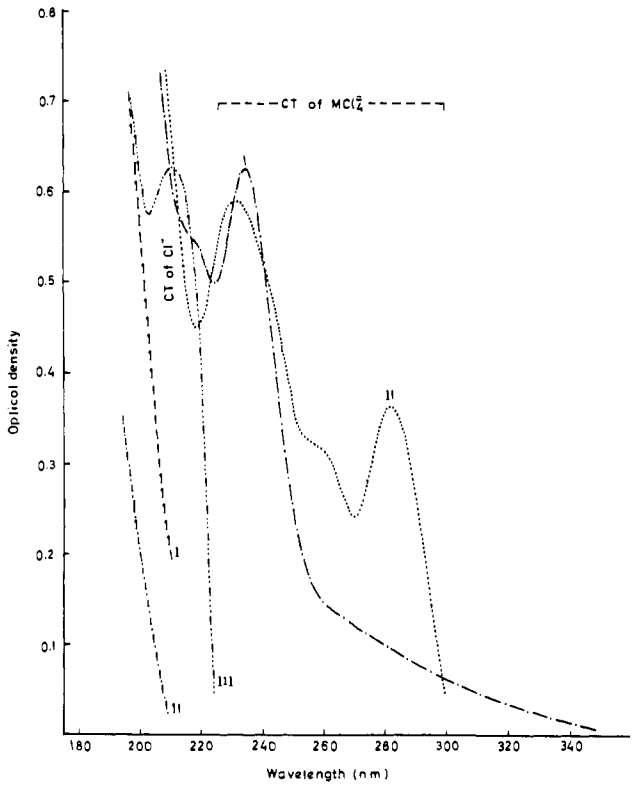

Figure 3. Charge-transfer spectra of MCl_4^{2-} and Cl^- in MCl_2 (M = I, Co, II, Ni; and III, Mn) -rich mixtures of molten $(C_4H_9)_4N^+Cl^-$.

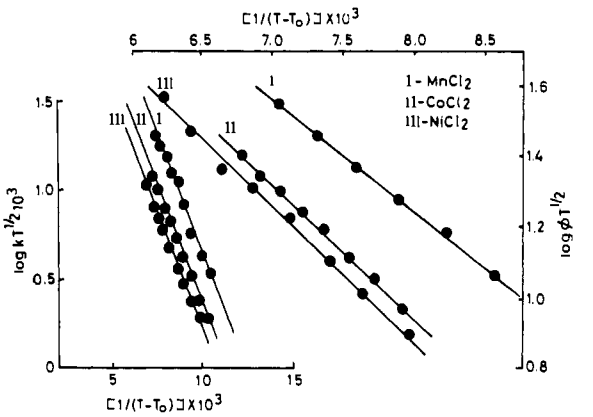

Figure 4. Plots of log $YT^{1/2}$ vs. $1/(T - T_0)$ for MCl_2-rich mixtures of molten $(C_4H_9)_4N^+Cl^-$.

$NiCl_2Br_2^{2-} > NiBr_4^{2-} > NiCl_2I_2^{2-} > NiI_4^{2-}$ is consistent with the decrease in B and $OE_{[X]}$ values from chloride to iodide.

CT Spectra of X^- in Thin Film of MX_2-Rich Mixtures of $R_4N^+X^-$. In addition to the CT spectra of MX_4^{2-} (Figure 3), still more intense bands at higher energies have been recorded for X^- as the ratio of $[(R_4N^+)_2MX_4^{2-}]$ to $[X^-]$ increases in the MX_2-rich mixtures of $R_4N^+X^-$ and are unaffected by the viscous medium containing the species of the type $\{(R_4N^+)_2MX_4^{2-}\}_x$ (M = Mn, Co, and Ni) for a given X^-. The band separation of 0.87 to 0.97 eV in iodide is comparable[33,34] with the calculated value of 0.889 eV for the doublets in transitions to $p^5\gamma_1$ configuration. The splitting of the doublet in Cl^- being 0.103 eV is too small to be observed (Figure 3). The CT bands of X^- may be assigned[31,33] either to $X^-np^5(n + 1)S \leftarrow Xnp^6$ or (Xnp^5 + a quasi-continuum of delocalized states of one electron) $\leftarrow Xnp^6$, $p^5\gamma_1 \leftarrow p^6\gamma_4$ transitions.

II. Transport Behavior. Free-Volume Model for the Electrical Conductances and Viscosities of Glass-Forming Melts. The transport properties have frequently been described by the rate process theory.[35,36] However, the electrical conductances and fluidities of molten mixtures of MCl_2 and $R_4N^+X^-$ measured as functions of temperature and composition show a non-Arrhenius type behavior and are therefore least-squares fitted to several functional forms based on the free-volume model.[11-17] The computed parameters are listed in Table VII. It is significant that the T_0 values are found to be independent of the method employed in

Table VIII. Energies of Activation of Conductances and Fluidities for MX_2-Rich Mixtures of R_4N^+X at Several Temperatures

T, °K	$\alpha RT^2 + {}^1/_2 RT$,[a] kcal/mol	E_{k,ϕ^1}	E_{k,ϕ^2}, kcal/mol[b]	E_{k,ϕ^3}	$E_{corr(\Lambda,\phi)}$, kcal/mol	E_η/E_Λ
		System: $(C_4H_9)_4N^+Cl^- + MnCl_2$ (24.5 mol %)				
373	0.540	15.02	15.20	16.00	15.95	
378	0.550	14.84	14.47	14.47	15.14	
383	0.560	14.25	13.81	13.71	14.48	
388	0.570	13.52	13.21	12.80	13.75	
393	0.580	12.78	12.66	12.56	13.25	1.333
	(0.391)[a]	(17.37)[c]	(17.84)	(16.59)	(17.66)	
398	0.591	12.09	12.16	12.17	12.73	1.256
	(0.395)	(15.61)	(15.97)	(15.22)	(16.00)	
403	0.601	11.47	11.70	11.42	12.13	1.238
	(0.400)	(14.24)	(14.42)	(15.21)	(15.02)	
408	0.612	10.91	11.27	10.65	11.55	1.168
	(0.405)	(13.15)	(13.12)	(12.98)	(13.49)	
413	0.623	10.41	10.88	10.28	11.15	1.138
	(0.410)	(12.26)	(12.01)	(12.57)	(12.69)	
418						
	(0.415)	(11.52)	(11.06)	(11.66)	(11.83)	
423						
	(0.420)	(10.89)	(10.23)	(11.24)	(11.21)	
428						
	(0.425)	(10.36)	(9.51)	(10.51)	(10.55)	
		System: $(C_4H_9)_4N^+Cl^- + CoCl_2$ (26.58 mol %)				
373	0.538	17.97	18.33	18.28	18.73	
378	0.548	17.17	16.72	17.83	17.83	
383	0.558	17.05	16.14	15.22	16.70	
388	0.568	15.92	15.22	14.85	15.90	
393	0.578	14.82	14.40	13.71	14.89	
398	0.589	13.82	13.66	12.79	14.01	1.329
	(0.395)	(17.97)	(18.43)	(18.28)	(18.62)	
403	0.599	12.93	12.99	11.42	13.05	1.354
	(0.400)	(17.29)	(17.26)	(17.28)	(17.68)	
408	0.610	12.17	12.39	10.51	12.30	1.352
	(0.405)	(16.33)	(16.23)	(16.13)	(16.64)	
413	0.621	10.50	11.84	9.69	11.30	1.385
	(0.410)	(15.34)	(15.30)	(15.08)	(15.65)	
418						
	(0.415)	(14.41)	(14.47)	(14.62)	(14.92)	
423						
	(0.420)	(13.57)	(13.73)	(13.71)	(14.09)	
428						
	(0.425)	(12.82)	(13.05)	(12.98)	(13.38)	
433						
	(0.430)	(12.16)	(12.44)	(12.11)	(12.67)	
		System: $(C_4H_9)_4N^+Cl^- + NiCl_2$ (22.13 mol %)				
373	0.521	17.79	18.02	18.28	18.55	
378	0.530	16.39	16.80	17.37	17.38	
383	0.540	15.08	15.73	15.99	16.14	
388	0.550	13.94	13.78	14.85	15.07	
393	0.559	12.96	13.94	13.71	14.10	1.373
	(0.391)	(19.73)	(19.07)	(18.46)	(19.36)	
398	0.569	12.13	13.18	12.80	13.27	1.341
	(0.395)	(17.53)	(17.42)	(17.27)	(17.80)	
403	0.579	11.41	12.49	11.99	12.54	1.313
	(0.400)	(16.00)	(16.01)	(16.13)	(16.47)	
408	0.588	10.80	11.19	11.43	11.73	1.306
	(0.405)	(14.73)	(14.79)	(15.21)	(15.16)	
413	0.598	10.27	11.33	10.65	11.35	1.247
	(0.410)	(13.67)	(13.73)	(13.85)	(14.16)	
418						
	(0.415)	(12.79)	(12.80)	(13.16)	(13.33)	
423						
	(0.420)	(12.04)	(11.98)	(12.68)	(12.65)	
428						
	(0.425)	(11.39)	(11.26)	(11.52)	(11.82)	

[a] ${}^1/_2 RT$ is added to $\langle E_\phi \rangle$. [b] E_{k,ϕ^1} from the derivative of $a + bt + ct^2$; E_{k,ϕ^2} from the derivative of $a \exp[-b/(T-c)]$ and E_{k,ϕ^3} from the slope of Arrhenius plot log (k, ϕ) vs. $1/T$. [c] E_ϕ values are given in parentheses.

studying the transport behavior as $T_{0,\Lambda} = T_{0,\phi}$ (Table VII). Thus the plots of log $Y(k,\phi)$ vs. $1/T$ become linear by the introduction of a third adjustable parameter, T_0 as shown in the plots (Figure 4) of log $YT^{1/2}$ vs. $1/(T - T_0)$.

The energies of activation, $E_{k,\phi}$, were evaluated from the derivatives d ln Y/d(T^{-1}) by making use of the three parameter equations (Table VII) for the transport behavior, and also from the successive pairs of points at 5° intervals from the plots of log Y vs. $1/T$. The plot of the averages of $E_{k,\phi^1} + E_{k,\phi^2} + E_{k,\phi^3}$ as a function of composition shows

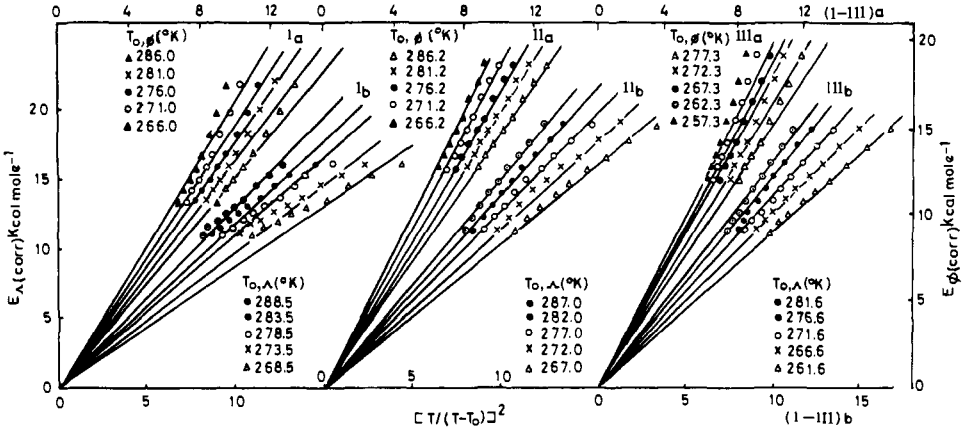

Figure 5. Test of results for sensitivity to T_0 of $E_{corr(\Lambda,\phi)}$ vs. $[T/(T - T_0)]^2$ plots for MCl_2-rich mixtures of molten $(C_4H_9)_4N^+Cl^-$.

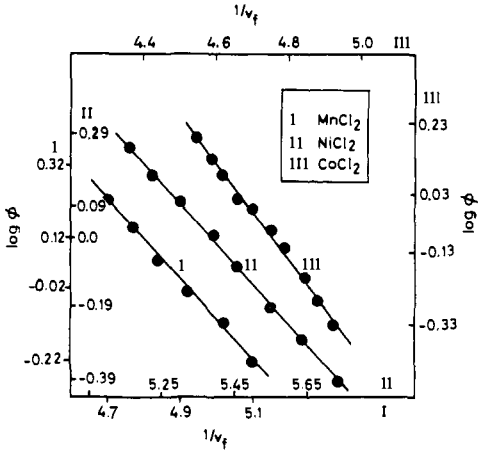

Figure 6. Plots of log ϕ vs. $1/v_f$ for MCl_2-rich mixtures of molten $(C_4H_9)_4N^+Cl^-$.

that $E_{k,\phi}$ is composition independent in the cases of dilute solutions unlike those in the glassy material. The energies of activation have been found to increase considerably at low temperatures and decrease slowly with an increase in temperature (Table VIII). The corrected activation energies, $E_{corr(\Lambda,\phi)}$, were calculated from the expressions $E_{corr(\Lambda)} = \alpha RT^2 + (\frac{1}{2})RT + \langle E_k \rangle$ and $E_{corr(\phi)} = \frac{1}{2}RT + \langle E_\phi \rangle = k_\phi R[T/(T - T_0)]^2$, respectively, using the $\langle E_{k,\phi} \rangle$ values and the coefficient of cubical expansion, α, evaluated at several temperatures from the density data expressed by the least-squares fit

$$\rho_I = 1.1975 - 0.58099 \times 10^{-3}(T)$$

$$\rho_{II} = 1.2006 - 0.58397 \times 10^{-3}(T)$$

$$\rho_{III} = 1.1894 - 0.5208 \times 10^{-3}(T)$$

for (I) $MnCl_2 + (C_4H_9)_4N^+Cl^-$, (II) $CoCl_2 + (C_4H_9)_4N^+Cl^-$, and (III) $NiCl_2 + (C_4H_9)_4N^+Cl^-$, respectively. The applicability of the free-volume model in explaining the transport behavior of the glass-forming melts under discussion is further supported by the linear plots (Figure 5) of E_{corr} vs. $[T/(T - T_0)]^2$ as expected on the basis of the equation, $E_{corr} = A[T/(T - T_0)]^2 + B$ based on such a model.

An increase in $E_{corr(\phi)}$ with a decrease in temperature (Table VIII) as well as an increase in $[MX_2]$ in molten $R_4N^+X^-$ suggests the presence of increased molecular association/intermolecular forces[37] as apparent from an approximately constant ratio of E_η/E_Λ and the nonlinear plots of viscosity, η vs. $[MX_2]$.

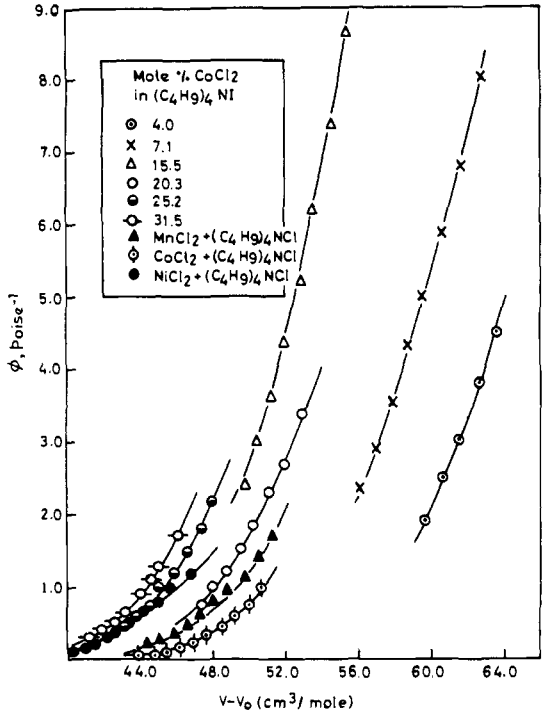

Figure 7. Plots of ϕ vs. $v - v_0$ for MCl_2-rich mixtures of molten $(C_4H_9)_4N^+X^-$.

The applicability of the free-volume model to these systems is further supported by the linear plots of T_0 vs. cationic potential.[38,39] T_0 has been found to decrease with successive increases in $[CoCl_2]$ as a result of complex formation which leads to an eventual supercooling to glassy states. At low temperatures the association of such species $\{(R_4B^+)_2MCl_2X_2^{2-}\}_x$, in which x depends on the polymeric tendency of these species, results in a highly viscous liquid. This view may also be supported by a high E_η, and the low electrical conductances.

The linear plots of log ϕ vs. $1/v_f$ (Figure 6) for $MX_2 + R_4N^+X^-$ justify the applicability of Doolittle's expression based on the free-volume model. Similar expressions[40] have recently been used in explaining the fluidities as a function of free volume, v_f. For example, Hildebrand's equation $\phi = B(v - v_0)/v_0$ has been found suitable in few systems since volume expansion has been mentioned as the primary cause for the ease of viscous flow. Linear plots of ϕ vs. $(v - v_0)$ and ϕ vs. $(v - v_0)/v_0$ have been reported[40] in different ranges of temperature. However, in the present investigations the plots of ϕ vs. $(v - v_0)$ are linear only in the high-

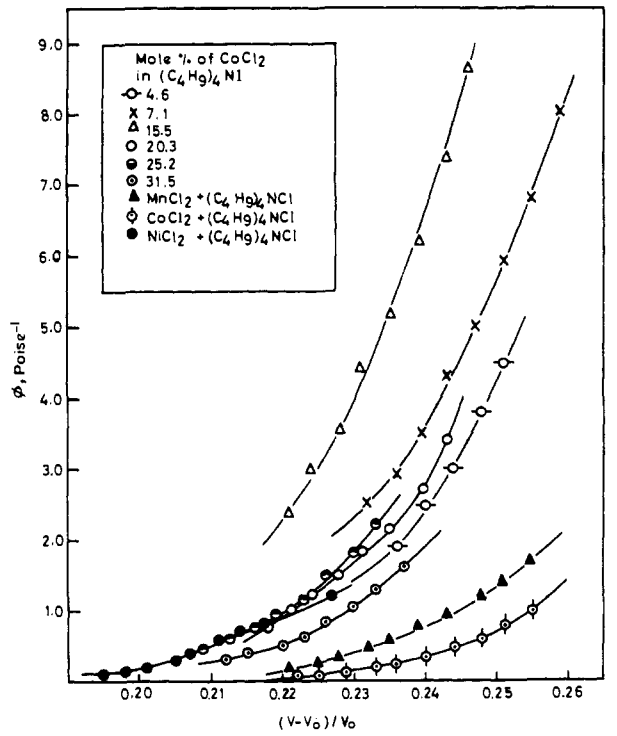

Figure 8. Plots of ϕ vs. $(v - v_0)/v_0$ relative volume expansion for MCl_2-rich mixtures of molten $(C_4H_9)_4N^+X^-$.

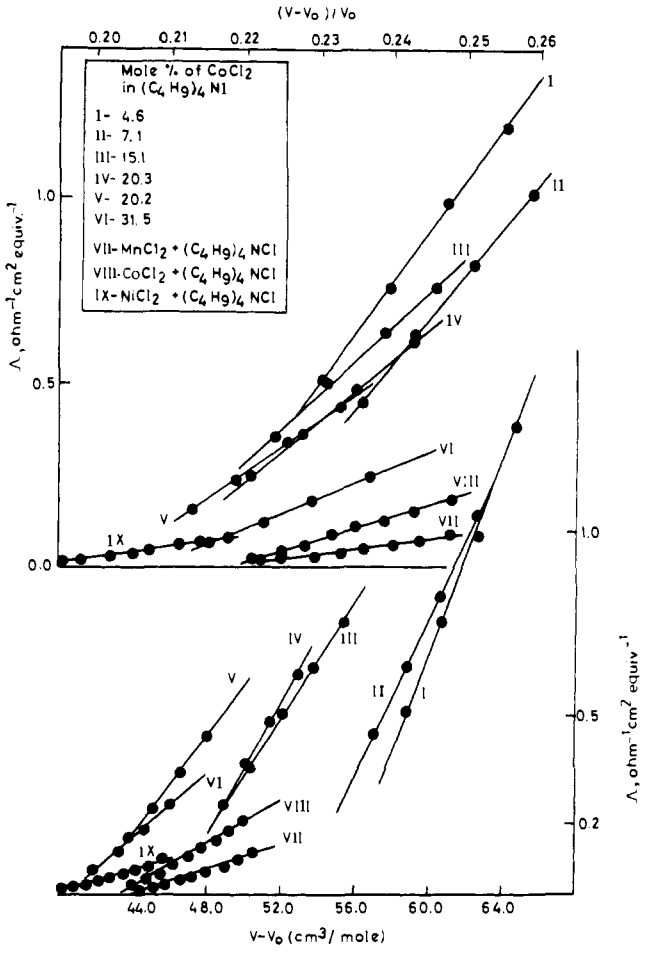

Figure 9. Plots of Λ vs. $v - v_0$ and $(v - v_0)/v_0$ for MCl_2-rich mixtures of molten $(C_4H_9)_4N^+X^-$.

temperature range, i.e., much above the melting points of the systems. On the other hand, the viscosity measurements were possible even at temperatures lower than those in the corresponding dilute solutions as the melts become soft with successive increases in $[MX_2]$. The plots of ϕ vs. $(v - v_0)$ are found to be nonlinear (Figure 7) presumably because of much increased molecular interactions/associations. Similar behaviors are shown by these systems in the plots of ϕ vs. $(v - v_0)/v_0$ (Figure 8). In such cases the molecules are expected to be closely packed and the linear relation between the fluidity and molal volume is violated.[40] The viscosity anomalies at lower temperatures have earlier been ascribed to a scarcity of free space which does not permit free rotation of molecules in the liquid. This may lead to the formation of "clusters" or "network"-like arrangements" due to the increased intermolecular forces.

However, the electrical conductances of ionic melts may be explained satisfactorily by the expression, $\Lambda = B_\Lambda[(v - v_0)/v_0]$, as shown in Figure 9, for several systems. This may lead to the assumption that the mechanism of ionic conductance is presumably different from that of viscosity, as the former involves the exchange of ions with the free volume while the latter has to overcome a potential energy barrier in laminar flow of clusters.

Acknowledgment. It is a pleasure to thank Dr. Pedro Smith of Oak Ridge National Laboratory for helping us in computer programming, and Professors B. R. Sundheim and Wasi-ur-Rahman of New York University and Head of the Department of Chemistry, Aligarh Muslim University, respectively, for providing the necessary facilities. Financial assistance to three of us (M.R.I., S.A., and B.W.) from the C.S.I.R. (New Delhi) is gratefully acknowledged.

References and Notes

(1) G. P. Smith, C. H. Liu, and T. R. Griffiths, *J. Am. Chem. Soc.*, **86**, 4796 (1964).
(2) G. P. Smith and S. von Winbush, *J. Am. Chem. Soc.*, **88**, 2127 (1966).
(3) N. Islam, *Aust. J. Chem.*, **26**, 2371 (1973).
(4) B. R. Sundheim and N. Islam, *Appl. Spectrosc.*, **27**, 285 (1973).
(5) B. R. Sundheim and N. Islam, *Appl. Spectrosc.*, **27**, 394 (1973).
(6) N. Islam, *Appl. Spectrosc.*, **28**, 277 (1974).
(7) N. Islam, B. Jamil, and S. A. A. Zaidi, *Indian J. Chem.*, **11**, 266 (1973).
(8) N. Islam and M. R. Islam, *Z. Phys. Chem. (Leipzig)*, **253**, 340 (1973).
(9) N. Islam and M. R. Islam, *Indian J. Chem.*, **12**, 705 (1974).
(10) A. D. Liehr and C. J. Ballhausen, *Ann. Phys. (N.Y.)*, **6**, 134 (1959).
(11) M. H. Cohen and D. Turnbull, *J. Chem. Phys.*, **31**, 1164 (1959).
(12) D. Turnbull and M. H. Cohen, *J. Chem. Phys.*, **29**, 1049 (1958); **34**, 120 (1961).
(13) C. A. Angell, *J. Phys. Chem.*, **70**, 3988 (1966); **68**, 1917 (1964); **68**, 218 (1964).
(14) C. T. Moynihan, *J. Phys. Chem.*, **70**, 3399 (1966).
(15) C. A. Angell, *J. Chem. Phys.*, **46**, 4673 (1967).
(16) C. A. Angell, *Aust. J. Chem.*, **23**, 929 (1970).
(17) A. J. Barlow, J. Lamb, and A. J. Matheson, *Proc. R. Soc. London, Ser. A*, **292**, 322 (1966).
(18) T. Moeller, *Inorg. Synth.*, **5**, 153 (1957).
(19) J. H. Kleinheksel and H. C. Kremers, *J. Am. Chem. Soc.*, **50**, 959 (1928).
(20) C. R. Boston and G. P. Smith, *J. Phys. Chem.*, **62**, 409 (1958).
(21) C. K. Jørgensen, *Mol. Phys.*, **1**, 410 (1958).
(22) D. M. Gruen and R. L. McBeth, *J. Phys. Chem.*, **63**, 393 (1959).
(23) C. R. Boston and G. P. Smith, *J. Am. Chem. Soc.*, **85**, 1006 (1963).
(24) D. M. Gruen and R. L. McBeth, *Pure Appl. Chem.*, **6**, 23 (1963).
(25) A. D. Liehr, *J. Phys. Chem.*, **67**, 1314 (1963).
(26) J. Ferguson, *J. Chem. Phys.*, **39**, 116 (1963).
(27) F. A. Cotton, D. M. L. Goodgame, and M. Goodgame, *J. Am. Chem. Soc.*, **83**, 4690 (1961).
(28) D. M. Gruen, *J. Inorg. Nucl. Chem.*, **4**, 74 (1957).
(29) D. M. Gruen, S. Fried, P. Graf, and R. L. McBeth, *Proc. U.N. Int. Conf. Peaceful Uses At. Energy, 2nd*, **12**, 112 (1958).
(30) N. Islam, *Appl. Spectrosc.*, to be published.
(31) C. K. Jørgensen, "Chemical Bonding Inferred from Visible and Ultraviolet Absorption Spectra" in "Solid State Physics", Vol. 13, F. Seitz and D. Turnbull, Ed., Academic Press, New York, N.Y., 1962, pp 375–462.
(32) C. K. Jørgensen, *Mol. Phys.*, **6**, 43 (1963).
(33) J. E. Eby, K. J. Teegarden, and D. B. Dutton, *Phys. Rev.*, **116**, 1099 (1959).
(34) R. S. Knox and N. Inchanspe, *Phys. Rev.*, **116**, 1093 (1959).
(35) G. J. Janz, *J. Chem. Educ.*, **39**, 59 (1962).
(36) H. Bloom, *Rev. Pure Appl. Chem.*, **9**, 139 (1959).
(37) W. Fieggen, *Recl. Trav. Chim. Pays-Bas*, **89**, 625 (1970).
(38) E. R. Nightangle, Jr., *J. Phys. Chem.*, **63**, 1381 (1959).
(39) N. Islam, M. R. Islam, S. Ahmad, and B. Waris, to be published.
(40) H. Ertl and F. A. L. Dallien, *J. Phys. Chem.*, **77**, 3007 (1973).